J. Fluid Mech. (2004), *vol.* 504, *pp.* 61–71.
DOI: 10.1017/S0022112004008250 Printed in the United Kingdom

Simulated polymer stretch in a turbulent flow using Brownian dynamics

By V. E. TERRAPON[1], Y. DUBIEF[2], P. MOIN[1,2], E. S. G. SHAQFEH[1,3] AND S. K. LELE[1]

[1]Mechanical Engineering Department, Stanford University, Stanford, CA 94305, USA

[2]Center for Turbulence Research, Stanford University, Stanford, CA 94305, USA

[3]Department of Chemical Engineering, Stanford University, Stanford, CA 94305, USA

(Received 23 August 2003 and in revised form 16 January 2004)

We examine the phenomenon of polymer drag reduction in a turbulent flow through Brownian dynamics simulations. The dynamics of a large number of single polymer chains along their trajectories is investigated in a Newtonian turbulent channel flow. In particular, the FENE, FENE-P and multimode FENE models with realistic parameters are used to investigate the mechanisms of polymer stretching. A topological methodology is applied to characterize the ability of the flow to stretch the polymers. It is found using conditional statistics that at moderate Weissenberg number *Wi* the polymers, that are stretched to a large fraction of their maximum extensibility, have experienced a strong biaxial extensional flow. When *Wi* is increased other flow types can stretch the polymers but the few highly extended molecules again have, on average, experienced a biaxial extensional flow. Moreover, highly extended polymers are found in the near-wall regions around the quasi-streamwise vortices, essentially in regions of strong biaxial extensional flow.

1. Introduction

Numerous studies of turbulent drag reduction by polymer additives have been performed since its first experimental observation by Toms (1948) and different mechanisms have been proposed (Lumley 1969; Tabor & De Gennes 1986; Sreenivasan & White 2000), but a conclusive explanation of the physics associated with the phenomenon is still lacking. Most of the recent numerical studies have focused on a continuum approach, i.e. solving a constitutive equation (Oldroyd-B, FENE-P) in an Eulerian frame of reference, e.g. Dimitropoulos, Sureshkumar & Beris (1998), Min *et al.* (2003), Dubief & Lele (2001), Sibilla & Baron (2002), Den Toonder *et al.* (1997). This has the advantage of allowing the polymer stress calculation at each grid cell; therefore the effect of the polymers on the flow can be determined. Many studies using this approach have shown significant drag reduction and the simulations reproduce qualitatively the results obtained experimentally. However, the accuracy of the constitutive equation has always been questioned, since it is either based on an unphysical model in the case of the Oldroyd-B or based on a closure approximation in the case of the FENE-P. Moreover, Dubief *et al.* (2004) have shown that the continuum calculations are affected by a lack of resolution in the low drag reduction regime limit, which prevents any conclusive explanation of the onset of drag reduction. This resolution problem due to small scales is generated by the advection term in the Eulerian representation which can be avoided by the use of a Lagrangian description.

The Lagrangian approach is also very useful in order to assess the models used in the Eulerian calculations, since it allows the use of more accurate models (FENE, FENE chain, bead–rod) as a representation of the polymer molecule. Moreover, the detailed mechanisms of polymer dynamics and the influence of the internal modes can be studied since the equations are solved for each polymer molecule along its trajectory.

Massah *et al.* (1993) have performed a Lagrangian simulation in a turbulent channel flow using an accurate bead–spring chain. They have shown that polymers can also unravel within the viscous sublayer if the Weissenberg number is large enough. Ilg *et al.* (2002) have compared the FENE and FENE-P models in wall turbulent flow and observed that polymers become highly oriented parallel to the mean flow direction and are characterized by a broad distribution of extensions. Stone & Graham (2003) demonstrated in a model of the turbulent buffer layer that stretching of the polymers is determined by the largest Lyapunov exponent for the velocity field and that polymers become highly stretched in the near-wall streaks and relax as they move into and around the streamwise vortex cores. Finally, Zhou & Akhavan (2003) have compared different models and shown that the dominant contributions to the polymer stress arise from patches of biaxial and uniaxial elongational flow encountered in the buffer layer. However, all these studies are based on a small number of different trajectories and they have therefore been based on limited statistical evidence.

In this study, the FENE dumbbell model is used to investigate the polymer dynamics in a turbulent channel flow. Terrapon *et al.* (2003) have demonstrated that the FENE chain, the FENE dumbbell and the FENE-P models give qualitatively similar results. This motivates the choice for the FENE dumbbell model since it is computationally less expensive than a bead–spring chain and reproduces accurately the polymer dynamics in a turbulent flow. However, a bead–spring chain model and the FENE-P model have also been used in one case in order to validate the present findings for other models. Unlike previous studies, a large ensemble of polymer molecules is used in order to sample the broad range of flow types present in a turbulent flow and a new method of statistical interpretation is introduced.

2. Models and numerical implementation

The Lagrangian description is based on tracking the centre of mass of a large ensemble of polymer molecules and solving the conformation equation for their extension vector along their trajectories. The Newtonian turbulent flow field is obtained from a direct numerical simulation of a channel flow.

The integration of the polymer molecule trajectories assumes that the molecule centre-of-mass motion is characterized by no inertia and an infinite Péclet number. Therefore, these trajectories represent an exact Lagrangian description of the flow. The equation for the position of their centre of mass is given by

$$\frac{\mathrm{d}\boldsymbol{x}}{\mathrm{d}t} = \boldsymbol{u}_p(\boldsymbol{x}), \tag{2.1}$$

where $\boldsymbol{u}_p$ is the velocity of the polymer molecule at its position $\boldsymbol{x}$ which needs to be interpolated from the velocity field. In this equation and throughout the paper all variables are made dimensionless with the centreline velocity U_c of the corresponding Poiseuille flow and the half-height h of the channel.

The Finitely Extensible Nonlinear Elastic (FENE) model is based on an elastic dumbbell which represents the polymer molecule as two beads connected by a

spring (Bird *et al.* 1987). The nonlinear spring force is modelled by a Warner spring representing the entropic forces which tend to bring the polymer back into its coiled configuration. The nonlinearity of the spring ensures that the dumbbell cannot extend more than a given maximum extension $q_{max} = \sqrt{b}$. The equation for the extension vector of the polymer is derived by neglecting the inertia of the beads and equilibrating the different forces acting on the beads, i.e. the drag force, the nonlinear spring force and the Brownian force representing the collision of the beads with the molecules of the solvent. After non-dimensionalization the equation for the end-to-end vector $\boldsymbol{q}$ of the dumbbell is

$$\frac{\mathrm{d}\boldsymbol{q}}{\mathrm{d}t} = \nabla \boldsymbol{u} \cdot \boldsymbol{q} - \frac{1}{Wi} \frac{\boldsymbol{q}}{2(1 - q^2/b)} - \frac{1}{\sqrt{Wi}} \frac{\mathrm{d}\boldsymbol{W}}{\mathrm{d}t}, \tag{2.2}$$

where the Wiener process $\boldsymbol{W}$ represents the Brownian contribution (note that a Wiener process is strictly speaking non-differentiable) and $\nabla \boldsymbol{u}$ is the velocity gradient tensor at the position of the centre of mass of the polymer molecule. Again the time t and the velocity gradient tensor are made dimensionless with U_c and h. The Weissenberg number $Wi = \lambda U_c / h$ is defined as the ratio of the relaxation time λ of the polymer to the characteristic time h/U_c of the flow. In wall units the Weissenberg number is defined as $Wi^+ = \lambda u_\tau^2 / \nu$ where u_τ and ν are respectively the friction velocity and the viscosity of the solvent.

The flow calculation is performed with an incompressible second-order finite-differences code on a staggered grid. The time advancement used is a third-order Runge–Kutta/Crank–Nicholson scheme (for more details see Dubief *et al.* 2004). Equations (2.1) and (2.2) are solved using a smaller time step than the time step used for the flow field calculation. Therefore, the velocity at the intermediate time steps is obtained by linearly interpolating two flow fields in time. The polymer molecule itself is advanced using a second-order Runge–Kutta scheme. Since the Eulerian velocity is only known on a grid network, a spatial interpolation is needed to determine the velocity at its current position. The trilinear interpolation was found to be sufficient (see Terrapon *et al.* 2003 for a more detailed discussion). Finally, the time integration of (2.2) uses a semi-implicit predictor–corrector scheme (Oettinger 1996; Somasi *et al.* 2002).

3. Topological methodology

As mentioned previously, the second term on the right-hand side of (2.2) corresponds to the spring force which tends to bring back the polymer molecule to its coil configuration. It opposes the tendency of the flow to stretch the polymer and ensures therefore a bounded extension. Its nonlinearity becomes important when it approaches its maximal extension. The third term on the right-hand side of (2.2) represents the Brownian motion and has a zero mean. This term only adds a stochastic character to the dynamics and becomes less important at high Wi. Thus the stretching of a polymer molecule is mainly driven by the first term on the right-hand side of (2.2), unless the polymer is sitting near regions of simple shear flow where Brownian motion and advection balance in the configuration dynamics. The use of the topological methodology introduced by Chong, Perry & Cantwell (1990) is motivated by the analogy of (2.2) and the equation for the flow patterns at a critical point

$$\frac{\mathrm{d}\boldsymbol{y}}{\mathrm{d}t} = \nabla \boldsymbol{u} \cdot \boldsymbol{y}, \tag{3.1}$$

where $\boldsymbol{y}$ determines the shape of the local flow field seen by an observer travelling with a fluid particle (like the polymer molecules in this case) and $\nabla \boldsymbol{u}$ is the velocity gradient

tensor. Equation (3.1) would represent the trajectories of the dumbbell beads in the absence of the spring and Brownian forces. Indubitably the entropic and Brownian forces alter this dynamics but since the spring force only constrains the stretching of the molecule, the unravelling of the polymer molecule is driven by the first term on the right-hand side of (2.2). Therefore, it is very instructive to analyse this term in more detail.

The topological methodology is based on the solutions of (3.1) rewritten in its canonical form. The flow topologies of an incompressible flow can then be classified according to the eigenvalues of the velocity gradient tensor (Chong *et al.* 1990; Blackburn, Mansour & Cantwell 1996). These eigenvalues define the three-dimensional flow type seen by a polymer molecule at its location. For an incompressible flow the eigenvalues, σ, are obtained as solutions of the characteristic equation

$$\sigma^3 + Q\sigma + R = 0, \tag{3.2}$$

with the tensor invariants Q and R given by

$$Q = -\tfrac{1}{2}\mathrm{tr}((\nabla \boldsymbol{u})^2), \tag{3.3a}$$

$$R = -\mathrm{det}(\nabla \boldsymbol{u}). \tag{3.3b}$$

The nature of the eigenvalues is determined by the discriminant $D = (27/4)R^2 + Q^3$. $D > 0$ gives rise to one real, two complex-conjugate eigenvalues; $D < 0$ gives three real distinct eigenvalues and $D = 0$ corresponds to three real eigenvalues of which two are equal. A further classification can be made according to the values of Q and R (see figure 2 in Blackburn *et al.* 1996), e.g. Q measures the difference between rotation and strain of the local flow. One can think of the imaginary part of the eigenvalues as a measure of the local rotational character of the flow, whereas the real part quantifies its extensional character, i.e. a negative/positive real part indicates respectively a compression/extension in the corresponding direction. Note that this classification does not give any information on the axis of extension/compression or on the planes of rotation, which are in general not orthogonal.

De Gennes (1974) postulated that the coil–stretch transition of a polymer molecule in a three-dimensional steady flow is determined by the positive real eigenvalues of the velocity gradient tensor. However, because the sum of the eigenvalues vanishes in an incompressible flow due to the continuity condition, a compression axis/plane is always associated with an extension plane/axis. Thus, in the case of $D > 0$, even if the real eigenvalue is negative (compression), the real part of the two other complex-conjugate eigenvalues is positive. Therefore, the motion induced by these complex eigenvalues involves both rotation from their imaginary part and an extensional character dictated by their real part. It follows that a flow with $D > 0$ and $R > 0$ in a (Q, R) plot (implying a negative real eigenvalue and two complex-conjugate eigenvalues with positive real parts) will unravel the polymer molecule at a sufficient high Weissenberg number as illustrated in figure 1. In this particular case, the stretching does not occur along a specific direction but along a rotating axis in the plane associated with the complex-conjugate eigenvalues. This shows that the stretching of the polymer is driven by the extensional character of the flow quantified by the positive real part of the eigenvalues. From this topological analysis, one can conclude that a polymer molecule will only fully unravel if it experiences a flow with a strong extensional character, i.e. one of the eigenvalues of the local velocity gradient

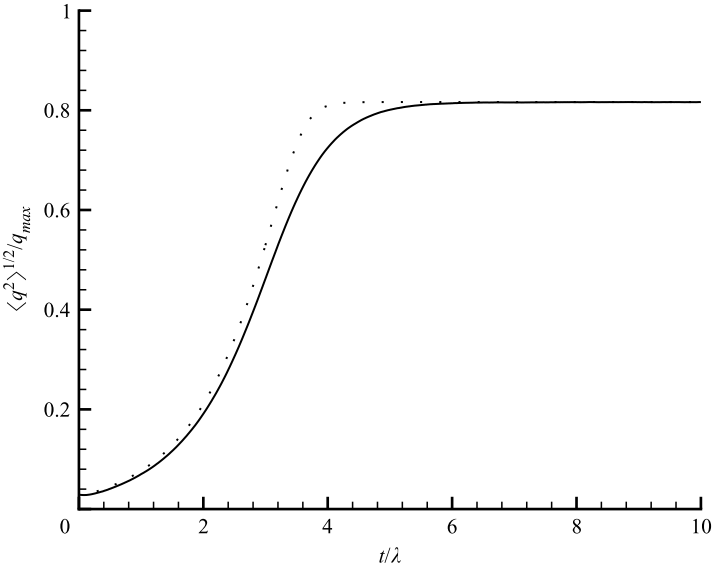

FIGURE 1. Normalized extension for a flow at $Wi = 3$ with $Q = 0.5$, $R = 1.25$ and $D = 10.67$ corresponding to the eigenvalues $\sigma_{1,2} = 0.5 \pm \mathrm{i}$ and $\sigma_3 = -1$; ——, FENE and · · · ·, FENE-P. $\langle \cdot \rangle$ represents the ensemble average.

tensor has a large positive real part. Therefore, we introduce

$$\sigma^* \equiv \max_i(\mathrm{Re}(\sigma_i)) \tag{3.4}$$

as a measure of the ability of the flow to stretch the polymer molecule.

A similar analysis for the two-dimensional case has already been proposed by Hur *et al.* (2002), who looked at the percentage of straining relative to the vorticity. According to this analysis, a shear flow can be seen as a limiting case, since it does not show a real coil–stretch transition but rather a tumbling dynamics as demonstrated by Smith, Babcock & Chu (1999) and Hur *et al.* (2001). This tumbling is caused by the Brownian motion which displaces extended molecules away from the extensional axis towards the compression axis, leading to a recoil of the molecule. Such tumbling dynamics can also be expected in a three-dimensional case when compression and extension axes are very close to each other.

These previous considerations are only based on the start-up of steady flows. In a turbulent flow, the velocity gradient tensor constantly changes with time, so that the application of the above analysis becomes more complicated. Not only is the flow type important but also its duration. Even a strong flow will not unravel a polymer molecule if it does not last long enough. Therefore, these considerations motivate the analysis of the flow topologies in a turbulent channel flow. Blackburn *et al.* (1996) have shown that the joint probability distribution function (PDF) of Q and R has a characteristic teardrop shape (see figure 2*a*). The isovalues of σ^* calculated from (3.4) are shown in figure 2(*b*). Combining these two plots indicates that strong events, i.e. large σ^*, are most likely to correspond to positive R, negative Q and negative D, i.e. biaxial extension.

4. Results

The Navier–Stokes equation is solved in a minimal channel (Jimenez & Moin 1991) at constant mass flux and a Reynolds number $Re = U_c h/\nu = 7500$, where ν is the

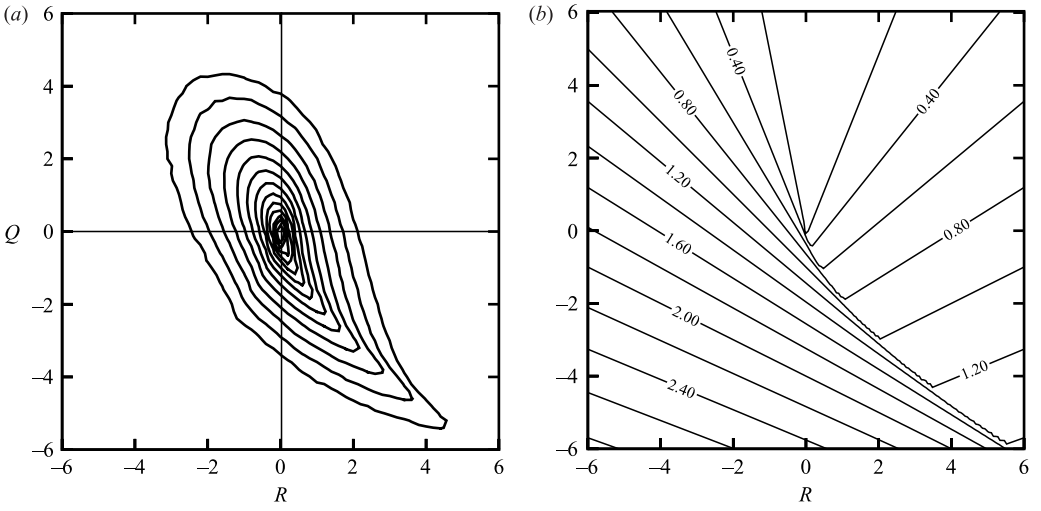

FIGURE 2. (*a*) PDF plots of Q *vs.* R in the buffer layer (exponential scale from 3.5×10^{-5} to 0.16); (*b*) isosurfaces of σ^* as a function of Q and R.

viscosity of the solvent. The channel is periodic in the x- and z-directions and has dimension $\pi h \times 2h \times h$. The simulation has been carried out on a grid of $96 \times 151 \times 64$ points giving a Reynolds number in wall units of $Re^+ = u_\tau h/\nu = 285$ (where u_τ is the friction velocity) so that $\Delta x^+ = 9.5$, $\Delta y^+ = 0.2 - 10$ and $\Delta z^+ = 4.5$. Finally a constant time step of $\Delta t = 0.01$ was chosen, ensuring a maximum $CFL = 0.6$. To achieve converged statistics, a large number of polymer molecules were needed. In this case $N_p = 10^5$ polymer molecules homogeneously distributed were used with each of them having a different trajectory. The extensibility parameter was chosen to be $b = 3600$ in order to simulate real molecules. Equation (2.2) was advanced using a time step $\Delta t_p = 0.001$, which is ten times smaller than that of the flow calculation, for a total time $T = 50.0$ after the transient part. Four different Weissenberg numbers were compared, i.e. $Wi = 1, 1.5, 3, 6$ and respectively in wall units $Wi^+ = 11, 16, 34, 68$. Note that each single polymer molecule experiences the same velocity gradients for all Weissenberg numbers.

Conditional statistics are used to investigate the stretching mechanisms. Statistics are gathered for all polymer molecules whose extension q normalized by the maximum extension q_{max} crosses a threshold value r. For each of these molecules the local σ^*, Q and R were recorded over a period of six time units before crossing the threshold r. Then these quantities are averaged over all the considered molecules as a function of the time Δt. In a first step an arbitrary threshold value $r = 0.65$ was chosen and statistics were gathered for different Wi. In a second step r was varied at a fixed $Wi = 3.0$. The results are summarized in figure 3. Note that the smallest threshold value chosen, i.e. $r = 0.65$, is larger than the mean extension found for a simple shear flow at the maximum Wi considered here. Therefore, the polymer molecules crossing this threshold can be considered as significantly extended. The mean value of σ^* is plotted in figure 3(*a, d*). One can see that at low Wi the polymer molecules experience a burst in σ^* just before reaching the threshold value. When Wi is increased, the maximum value of σ^* decreases (see figure 3*a*), as expected from § 3. Figure 3(*d*) illustrates that even at a larger Wi a large σ^* is needed to extend the polymer near to its maximum extension. Therefore, one can conclude that only rare strong events,

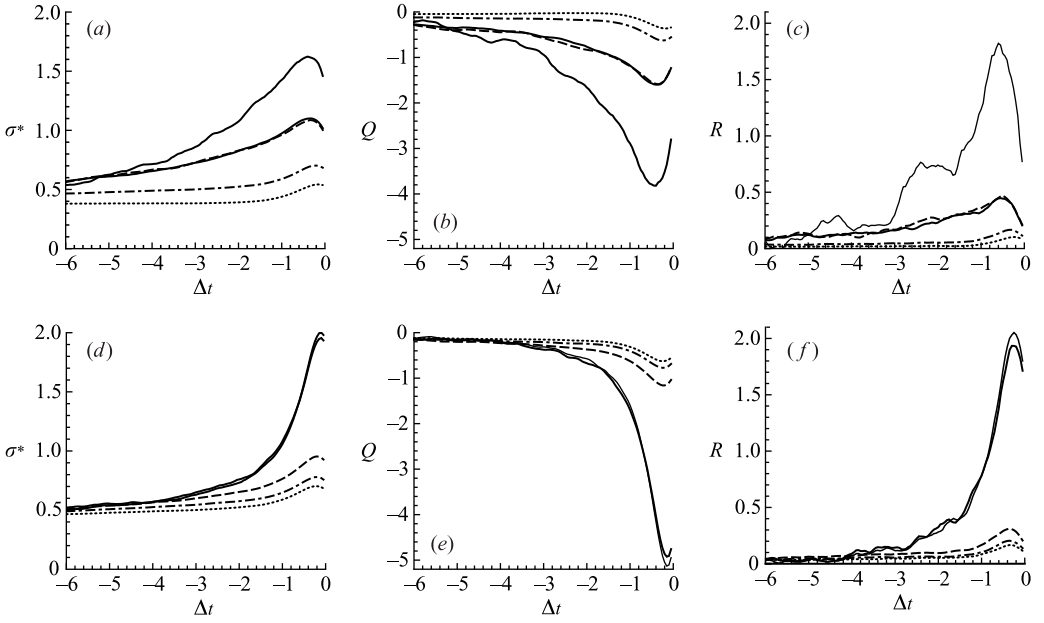

FIGURE 3. Conditional average of σ^*, Q and R for the polymer molecules crossing the threshold value $q/q_{max} = r$ as a function of the time Δt before crossing this threshold. (a,b,c) $r = 0.65$ and ——, $Wi = 1.0$; – – –, $Wi = 1.5$; — · —, $Wi = 3.0$; · · · ·, $Wi = 6.0$. (d,e,f) $Wi = 3.0$ and ——, $r = 0.95$; – – –, $r = 0.85$; — · —, $r = 0.75$; · · · ·, $r = 0.65$. Shown for comparison as a thin continuous line: $(a$–$c)$ results from a bead–spring chain with $N_b = 11$ beads at $Wi = 1.5$; $(d$–$f)$ results from the FENE-P model for $r = 0.95$.

i.e. large σ^*, can produce a large stretching of the polymer molecule at low Wi ; at high Wi weaker events are needed but a large σ^* is more efficient and achieves a larger extension of the polymer molecule. Figure 3(b,c,e,f) shows the conditional mean for Q and R. It is clear from these plots that, at low Wi, the extended molecules have experienced a strong biaxial extensional flow (see also figure 4 where one can see that D is on average negative, corresponding to three real eigenvalues and therefore to an extensional flow). This is also true at larger Wi for molecules near their maximum extension (see figure 3e,f). These results are in agreement with figure 2(a,b) which shows that the largest eigenvalues are rare events found at negative Q. It is also found (not shown here) that these strong events are in general characterized by a negative velocity gradient $\partial u/\partial x$, a negative streamwise velocity u and a positive wall-normal velocity v. It can therefore be deduced that these strong events are on average correlated with ejections of low-speed fluid away from the wall. Figure 4 shows the trajectory of the polymer molecules in a (Q,R) plot parametrized by the time Δt. All curves have a similar shape, which is a characteristic time evolution during the stretching process. A change in the Weissenberg number or the threshold value only affects the numerical values but the shape of the curve remains identical.

In order to demonstrate the generality of the previous results, similar conditional statistics have been gathered for the more accurate bead–spring chain model with $N_b = 11$ beads at $Wi = 1.5$ and for $r = 0.65$ and for the FENE-P model at $Wi = 3$ and for $r = 0.95$. The results are shown in figures 3$(a$–$c)$ and 3$(d$–$f)$ as a thin continuous line and agree very well with those from the FENE model. This clearly demonstrates

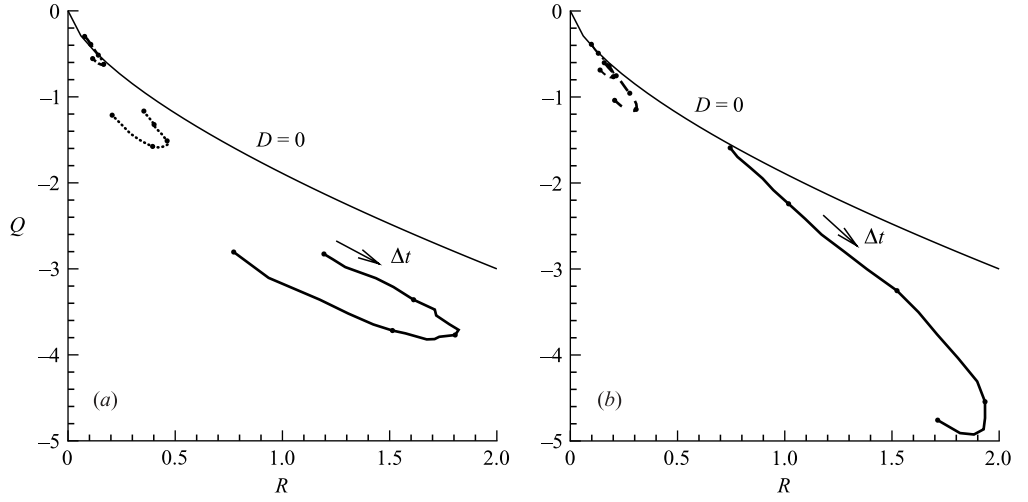

FIGURE 4. Mean time evolution of Q *vs.* R from $\Delta t = -1.0$ to $\Delta t = 0$. (*a*) $r = 0.65$ and ——, $Wi = 1.0$; – – –, $Wi = 1.5$; — · —, $Wi = 3.0$. (*b*) $Wi = 3.0$ and ——, $r = 0.95$; – – –, $r = 0.85$; — · —, $r = 0.75$. The dots correspond to time intervals of $\Delta t = 0.25$. The line $D = 0$ is also shown for comparison.

that the primary stretching mechanisms are the same for different models, even for models with many relaxation modes.

Dubief & Delcayre (2000) showed that vortices can be detected by positive isosurfaces of Q, where Q can also be computed as the difference between vorticity Ω and straining S. It is therefore interesting to note that polymer stretching is associated with negative values of Q, i.e. straining, whereas vortices are associated with positive values, i.e. rotation. Flow visualizations also demonstrate that the regions of large σ^* are always located next to the vortices and can also be seen as structures advected by the mean flow. This is illustrated in figure 5, which shows isosurfaces of Q representing the vortices, isosurfaces of σ^* and the polymer molecules which are highly stretched. The correlation between σ^* and the vortices is striking and can provide new insight into the mechanisms of polymer drag reduction. Dubief *et al.* (2004) have already shown by continuum calculations that polymers act on vortices by damping them. From the present results, it seems clear that the polymer is first stretched in these regions of large σ^* that are associated with the vortices.

As stated in the introduction, statistics were gathered in a Newtonian flow where the polymer molecules were considered passive. In a high drag reduction regime, polymers modify significantly the fluctuations of the turbulent velocity field. Therefore, similar statistics have also been collected in a non-Newtonian flow computed with the method of Dubief & Lele (2001) at drag reduction of approximatively 30%. The results were qualitatively similar to the Newtonian case. Moreover, it was verified that the joint probability distribution function of Q and R retains its characteristic teardrop shape even at high drag reduction. Thus, it can be inferred that the mechanisms of polymer stretching described in this paper are also valid for non-Newtonian flows. Lower polymer extensions and flow quantities were calculated since the fluctuations of the turbulent velocity field were significantly damped.

In terms of the onset of drag reduction, only very strong events can stretch the polymers at very low values of Wi. It is not obvious that a coil–stretch transition is necessary for the polymers to reduce drag but a sufficiently large extension is needed to

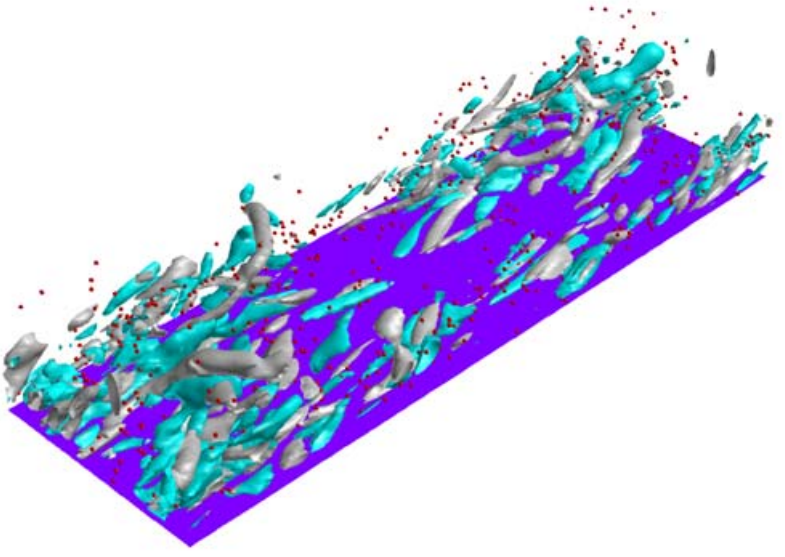

FIGURE 5. Instantaneous view of the lower half of the channel showing the isosurface $Q = 1.9$ (grey) representing the vortices, the isosurface (turquoise) of $\sigma^* = 1.6$ and the polymer molecules (red) with $q/q_{max} > 0.8$ at $Wi = 3$.

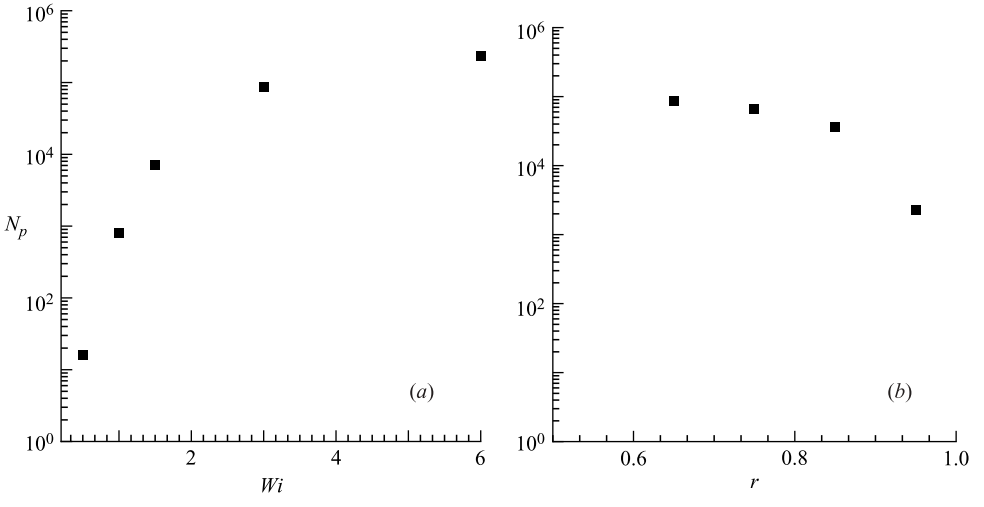

FIGURE 6. Number of polymer molecules having crossed $q/q_{max} = r$: (*a*) as a function of Wi for $r = 0.65$; (*b*) as a function of r for $Wi = 3.0$.

produce stress. Bird *et al.* (1987) showed that $Wi\sigma > 0.5$ must be satisfied for a coil–stretch transition to occur. This gives an absolute lower bound for the Weissenberg number $Wi_{cr} = 0.5\sigma^*_{max}$ below which no molecule can unravel. Assuming that drag reduction scales nearly linearly with the number of polymers stretching, one would see an important increase of drag reduction near what is apparently a critical Wi, since the number of molecules achieving a coil–stretch transition increases dramatically with Wi around this critical value (as illustrated in figure 6). This dramatic increase

of the number of stretched molecules can be understood by the distribution of flow types shown in figure 2(*a*), where the probability of finding weaker events increases exponentially.

5. Conclusions

Brownian dynamics simulations were used in a turbulent channel flow to investigate the mechanisms of polymer dynamics. Flow types were characterized according to the flow topologies and the quantity σ^* was introduced to measure the ability of the flow to stretch the polymer molecules. A large range of Weissenberg numbers were investigated and it was found that the polymers stretch primarily in straining flows in the near-wall region next to the vortices. At low Wi rare events of strong biaxial flows cause the chain to unravel whereas at higher Wi different flow types can stretch the polymer molecule, but only bursts of biaxial extensional flow can fully extend it. In summary, bursts of biaxial extensional flows, constrained by the flow topology, occuring approximately $0.5h/U_c$ before the maximum extension are the primary stretch mechanisms.

The authors would like to acknowledge the financial support provided by DARPA, Grant No. MDA972-01-C-0041.

REFERENCES

Bird, R., Curtiss, C., Armstrong, R. & Hassager, O. 1987 *Dynamics of Polymer Liquids*. 2nd Edn. Wiley.

Blackburn, H., Mansour, N. & Cantwell, B. 1996 Topology of fine-scale motions in turbulent channel flow. *J. Fluid Mech.* **310**, 269–292.

Chong, M., Perry, A. & Cantwell, B. 1990 A general classification of three-dimensional flow fields. *Phys. Fluids* A **2**, 765–777.

De Gennes, P. G. 1974 Coil-stretch transition of dilute flexible polymers under ultrahigh velocity gradients. *J. Chem. Phys.* **60**, 5030–5042.

Den Toonder, J., Hulsen, M., Kuiken, G. & Nieuwstadt, F. 1997 Drag reduction by polymer additives in a turbulent pipe flow: Numerical and laboratory experiments. *J. Fluid Mech.* **337**, 193–231.

Dimitropoulos, C., Sureshkumar, R. & Beris, A. 1998 Direct numerical simulation of viscoelastic turbulent channel flow exhibiting drag reduction: effect of the variation of rheological parameters. *J. Non-Newtonian Fluid Mech.* **79**, 433–468.

Dubief, Y. & Delcayre, F. 2000 On coherent-vortex identification in turbulence. *J. Turbul.* **1**(011), 1–22.

Dubief, Y. & Lele, S. 2001 Direct numerical simulation of polymer flow. *Annual Research Briefs, Center for Turbulent Research, Stanford University*, pp. 197–208.

Dubief, Y., Terrapon, V., White, C., Shaqfeh, E., Moin, P. & Lele, S. 2004 New answers on the interaction between polymers and vortices in turbulent flows. *Flow, turbulence and combustion* (submitted).

Hur, J., Shaqfeh, E., Babcock, H. & Chu, S. 2002 Dynamics and configurational fluctuations of single DNA molecules in linear mixed flows. *Phys. Rev.* E **66**, 011915.

Hur, J., Shaqfeh, E., Babcock, H., Smith, D. & Chu, S. 2001 Dynamics of dilute and semidilute DNA solutions in the start-up of shear flow. *J. Rheol.* **45**, 421.

Ilg, P., de Angelis, E., Karlin, I., Casciola, C. & Succi, S. 2002 Polymer dynamics in wall turbulent flow. *Europhys. Lett.* **58**, 616–622.

Jimenez, J. & Moin, P. 1991 The minimal flow unit in near-wall turbulence. *J. Fluid Mech.* **225**, 213–240.

Lumley, J. L. 1969 Drag reduction by additives. *Annu. Rev. Fluid Mech.* **1**, 367–384.

Massah, H., Kontomaris, K., Schowalter, W. & Hanratty, T. 1993 The configurations of a FENE bead-spring chain in transient rheological flows and in a turbulent flow. *Phys. Fluids* A **5**, 881–890.

Min, T., Yoo, J., Choi, H. & Joseph, D. 2003 Drag reduction by polymer additives in a turbulent channel flow. *J. Fluid Mech.* **486**, 213–238.

Oettinger, H. 1996 *Stochastic Processes in Polymeric Fluids.* Springer.

Sibilla, S. & Baron, A. 2002 Polymer stress statistics in the near-wall turbulent flow of a drag-reducing solution. *Phys. Fluids* **14**, 1123–1136.

Smith, D., Babcock, H. & Chu, S. 1999 Single-polymer dynamics in steady shear flow. *Science* **283**, 1724.

Somasi, M., Komami, B., Woo, N., Hur, J. & Shaqfeh, E. 2002 Brownian dynamics simulations of bead-rod and bead-spring chains: Numerical algorithms and coarse graining issues. *J. Non-Newtonian Fluid Mech.* **108**, 227–255.

Sreenivasan, K. & White, C. 2000 The onset of drag reduction by dilute polymer additives, and the maximum drag reduction asymptote. *J. Fluid Mech.* **409**, 149–164.

Stone, P. & Graham, M. 2003 Polymer dynamics in a model of the turbulent buffer layer. *Phys. Fluids* **15**, 1247–1256.

Tabor, M. & De Gennes, P. G. 1986 A cascade theory of drag reduction. *Europhys. Lett*. **2**, 519–522.

Terrapon, V., Dubief, Y., Moin, P. & Shaqfeh, E. 2003 Brownian dynamics simulation in a turbulent channel flow. *Proc. 4th ASME-JSME Joint Fluids Eng. Conf., Honolulu.*

Toms, B. 1948 Observation on the flow of linear polymer solutions through straight tubes at large Reynolds numbers. *Proc. Intl Rheological Congress* **2**, 135–141.

Zhou, Q. & Akhavan, R. 2003 A comparison of FENE and FENE-P dumbbell and chain models in turbulent flow. *J. Non-Newtonian Fluid Mech.* **109**, 115–155.